

# Halide-Salt-Free Synthesis of Silver Nanowires with High Yield and Purity for Transparent Conductive Films

Huaming Mao, Jie Chen, Linlin He, Zhengyang Fan, Yu Ren, Jungang Yin, Wei Dai, and Hongwei Yang\*

Cite This: *ACS Omega* 2023, 8, 7607–7614

Read Online

ACCESS |



Metrics &amp; More

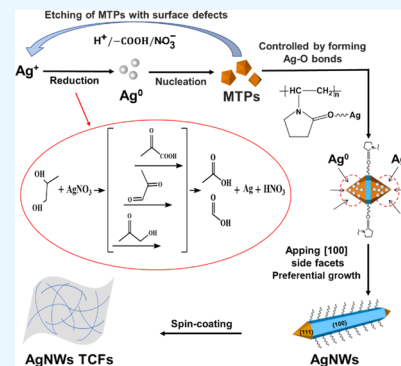


Article Recommendations



Supporting Information

**ABSTRACT:** To date, silver nanowires (AgNWs) are routinely synthesized. However, the controllable preparation of AgNWs without any halide salts has not reached a similar level. In particular, the halide-salt-free polyol synthesis of AgNWs commonly occurs above 413 K, and the property of AgNWs obtained is not so easy to control. In this study, a facile synthesis of AgNWs with a yield of up to ~90% in an average length of 75  $\mu\text{m}$  was successfully performed without any halide salts. The fabricated AgNW transparent conductive films (TCFs) show a transmittance of 81.7% (92.3% for the AgNW network only without substrate) at a sheet resistance of 12.25  $\Omega/\text{square}$ . In addition, the AgNW films show distinguished mechanical properties. More importantly, the reaction mechanism for AgNWs was briefly discussed, and the importance of reaction temperature, the mass ratio of poly(vinylpyrrolidone) (PVP)/AgNO<sub>3</sub>, and the atmosphere was emphasized. This knowledge will help enhance the reproducibility and scalability of polyol synthesis of high-quality AgNWs.



## 1. INTRODUCTION

AgNWs have attracted intense attention from both academia and industry because of their unique electronic, optical, and thermal properties. Due to their unique properties, AgNWs could have wide-range applications in biological sensors,<sup>1</sup> solar cells,<sup>2</sup> transparent conductive devices,<sup>3</sup> electronic skins,<sup>4</sup> and nanomedicine.<sup>5</sup> In recent years, various electronic equipments have gradually developed for refinement and artificial intelligence, raising higher-quality requirements on AgNWs. For example, Amjadi et al.<sup>6</sup> developed new types of strain sensors with high sensitivity, stretchability, and stability with a simple and low-cost fabrication process based on the sandwich-structured AgNW-PDMS nanocomposite. The tunable gauge factors and stretchability of the sensors are in the ranges of 2–14 and 70%, respectively, both of which are higher than those of the conventional strain sensors. Significant research on the synthesis method of AgNWs has been done to meet specific requirements of various application fields.

Some of the effective synthesis methods include polyol method, seeded method, template method, wet chemical method, and electrochemical reduction method. Recently, researchers have successfully prepared AgNWs of different sizes through the above methods. Remarkably, so far, many reports have shown that introducing traces of halide salts or inorganic derivatives (e.g., NaCl, CuCl<sub>2</sub>, FeCl<sub>3</sub>, Na<sub>2</sub>S, benzoin, etc.) is an important factor in determining the structural properties of AgNWs.<sup>7–9</sup> Although the methods of adding halide salts or inorganic derivatives are conducive to increasing the aspect ratio of AgNWs, this synthesis strategy is often accompanied by a high yield of silver nanoparticles (see Table S1). To obtain a pure AgNW dispersion, the reaction product

must be purified through a cumbersome process; for example, acetone, chloroform, or cyclohexane was added to the AgNW solution to regulate the polarity of the solution, and then AgNWs and nanoparticles were separated by centrifugation, filtration, decantation, or sedimentation, which results in the low yield of final products and the high production cost of AgNWs. For example, Chen et al.<sup>10</sup> reported that positive-pressure filtration could endow effective removal of small NPs from raw AgNWs. The filtered and redispersed AgNW dispersion was fixed on a rotary shaker and shaken at the speed of 75 rpm, followed by titration with acetone at a rate of 100–200 mL/s. After settling for 10 min, the supernatant was pipetted out. Thereafter, the flocculate was redispersed in 30 mL of 0.5 wt % PVP and five to seven cycles should be conducted to remove NPs and NRs.

Furthermore, the obtained AgNWs have shortcomings in some application fields, such as optoelectronics, biological sensors, and biomedical materials. This is because the halogen or metal ions contained in the halide salt will be adsorbed on the silver crystal plane or lattice during the growth of AgNWs. Also, it is difficult to completely remove the halogen or metal ions in the AgNW washing treatment, which will affect the electrical conductivity, thermal conductivity, and biocompat-

Received: November 7, 2022

Accepted: January 26, 2023

Published: February 14, 2023



ibility of the materials.<sup>11–15</sup> For example, in the as-prepared conductive microtextile and medical gauze sensors, the residual halogen or metal ions in AgNWs can reduce sensor sensitivity and stability. In addition, halogen is very sensitive to humidity, temperature, light, and electrical stress. If residual halogen in AgNWs is exposed to the air for a long time, it will increase corrosiveness and reduce the service life of the material.<sup>16–19</sup> For example, in the as-prepared flexible displays, the residual halogen or metal ions in AgNWs can reduce the service life of the flexible displays due to prolonged exposure to sunlight. Therefore, to eliminate the bad influence of halide salts on the synthesis and use of AgNWs, direct preparation of AgNWs without any halide salts is one of the most effective and feasible methods at present.

Currently, the polyol method is the most common method to synthesize AgNWs without halide salts. For example, Wu et al.<sup>20</sup> synthesized AgNWs with a width of about 200 nm from silver nitrate and PVP at a temperature of 433 K. The addition of silver nitrate and PVP was controlled by syringes. They proposed that the syringe rate and the molar ratio of PVP/AgNO<sub>3</sub> were important conditions to produce AgNWs. Jia et al.<sup>21</sup> fabricated AgNWs with a small diameter of 40 nm and a length of 10 μm using a mixed solvent of ethylene glycol (EG) and glycerol at a temperature of 473 K in the presence of PVP. They believed that the yield of the AgNWs was dependent on the viscosity and reduction ability of solvents. Cong-Wen et al.<sup>22</sup> reported the method of synthesizing AgNWs in 1,2-propylene glycol (1,2-PG) at temperatures of 413 K. The synthesized AgNWs had a length ranging from 2 to 20 μm and a diameter varying from 100 to 400 nm. However, the sample contained a mixture of relatively thick nanowires (250 nm in diameter and 2–5 μm in length). In addition, the synthesis of Ag seeds needs to be controlled. Although AgNWs can be prepared successfully now in a halide-salt-free method. For example, in the method introduced by Madeira et al.,<sup>23</sup> AgNWs were synthesized in a three-neck bottom flask. At a temperature of 413 K, AgNO<sub>3</sub> dissolved in 1,2-propanediol and PVP dissolved in 1,2-propanediol are simultaneously injected dropwise into the three-neck bottom flask. The sample contained a mixture of nanoparticles. The final solution needed to be purified several times.

In this work, for the first time, the AgNWs, made of silver nitrate (AgNO<sub>3</sub>) as a precursor, 1,2-PG as a reducing agent, and a solvent, were fabricated at a temperature of 393 K with high yield and purity. No halide salts were used and only PVP was adopted as a surface capping agent to inhibit the Ag atom growth on the {100} planes. More importantly, the synthesis mechanism of AgNWs was discussed in detail. Further, the obtained AgNWs were used to manufacture transparent conductive films, and their performances were discussed.

## 2. MATERIALS AND METHODS

**2.1. Materials.** Silver nitrate (AgNO<sub>3</sub>) was purchased from Sigma-Aldrich. PVP (K90) (Mn ≈ 1,300,000) was purchased from Aladdin Chemicals. 1,2-PG, hydroxyethyl cellulose (HEC, Dow-QP-100MH), and ethanol were purchased from Sinopharm Chemical Reagent Co. All chemicals, solvents, and reagents were of analytical grade.

**2.2. Synthesis of Silver Nanowires.** For a typical synthesis, 0.06 g of PVP (K90, MW ≈ 1,300,000) was dissolved in 50 mL of the 1,2-PG solution at a temperature of 298 K. Meanwhile, 1 g of AgNO<sub>3</sub> was dissolved in 50 mL of 1,2-PG at a temperature of 298 K. Two kinds of solutions were

then mixed together at a temperature of 298 K. The mixed solution was further stirred for uniformity and then transferred into a 200 mL Teflon-lined autoclave and heated in an oven at a temperature of 393 K for 6 h. After that, the autoclave was air-cooled to room temperature unaided. The resulting sample was rinsed with deionized water and centrifuged at 2000 rpm to remove the extra PVP and 1,2-PG. The as-prepared sample was then redispersed in ethanol for further characterization.

**2.3. Preparation of AgNW Transparent Conductive Films.** The AgNW suspension was diluted to 1.5, 2, 2.5, and 3 mg/mL with ethanol (≥99.0%). Then, HEC (15 wt %) was added to the diluted suspensions. Next, transparent conductive films of AgNWs were prepared by performing the spin-coating method at 600 rpm on the PET substrate. The coated AgNW films were subsequently placed in the drying oven at a temperature of 393 K for 30 min to improve the wire–wire contact points.

**2.4. Characterization.** The morphology and microstructure of the as-prepared AgNWs were characterized by SEM (FEI–Versa3D) and TEM (Tecnai G2-TF30), respectively. The crystalline phases of the as-synthesized AgNWs were analyzed by X-ray diffraction (XRD, Rigaku D/Max-3B, a scanning speed of 0.02° min<sup>-1</sup>) with Cu Kα radiation (λ = 1.54 Å) in the 2θ range from 20 to 90°. The UV–vis absorption spectra were obtained on a UV–vis spectrophotometer (PERSEE Genera TU-1901). To evaluate the oxidative products of 1,2-PG, the FTIR of the liquid phase test before and after the reaction was obtained by liquid IR cell and FTIR beam (Bruker IFS 66 v/S). FTIR measurement was carried out after the separation of AgNWs from the liquid phase. The transmittance of AgNW-based TCFs was obtained on a transmittance haze tester (SGW-820). The sheet resistance of AgNW TCFs was measured using a four-point probe method (SB100A/2).

## 3. RESULTS AND DISCUSSION

**3.1. Characterization of the Synthetic Silver Nanowires.** The reaction temperature and PVP should play effective roles in the synthesis of AgNWs. We thus discussed the effects of reaction temperature and PVP/AgNO<sub>3</sub> mass ratio on AgNWs by keeping all other parameters constant. The SEM images of the as-prepared samples are shown in Figures S1 and S2. Under the condition of the mass ratio of PVP/AgNO<sub>3</sub> of 6%, when the reaction temperature was 383 K, the AgNWs have an average length of 30 μm and an average diameter of 500 nm (Figure S1a,b). The yield of AgNWs was about 60%. A mixture of AgNWs, nanorods, and quasi-spherical nanoparticles was formed in the product. When the reaction temperature was 393 K, the average length of the AgNWs was 75 μm and the average diameter of the AgNWs was 220 nm (Figure S1c,d). The yield of AgNWs was about 90%. By contrast, as the reaction temperature increased up to 403 K, it is clear that the average length of the AgNWs was only 25 μm and the average diameter of AgNWs was 200 nm (Figure S1e,f). The yield of AgNWs was about 75%. A mixture of Ag nanowires and nanorods is formed in the product. Therefore, the optimal reaction temperature of AgNO<sub>3</sub> was 393 K. The SEM images of AgNWs prepared under different mass ratios of PVP/AgNO<sub>3</sub> are shown in Figure S2. It can be seen from the images that when the mass ratios of PVP/AgNO<sub>3</sub> were 5 and 7%, the corresponding average lengths of AgNWs were 25 and 50 μm and the corresponding average diameters of AgNWs were 480 and 180 nm. The yield of AgNWs in the two samples

was about 80%. It was apparent that AgNWs have the finest length and diameter when the mass ratio of PVP/AgNO<sub>3</sub> was 6%. Therefore, 6% was determined as the optimum mass ratio of PVP/AgNO<sub>3</sub>. The reaction temperature (393 K) and the PVP/AgNO<sub>3</sub> mass ratio (6%) were determined as the best conditions by comparing the yield, length, and diameter of the AgNWs in the as-prepared samples. The following discussion is thereby based on these conditions.

In this work, we used 1,2-PG as a reducing agent and PVP as a dispersant. The final gray-white product was obtained after synthesis, for which the yield of AgNWs was over 90%. SEM images obtained from the as-prepared samples are shown in Figure 1. From Figure 1a,c, it could be seen clearly that the

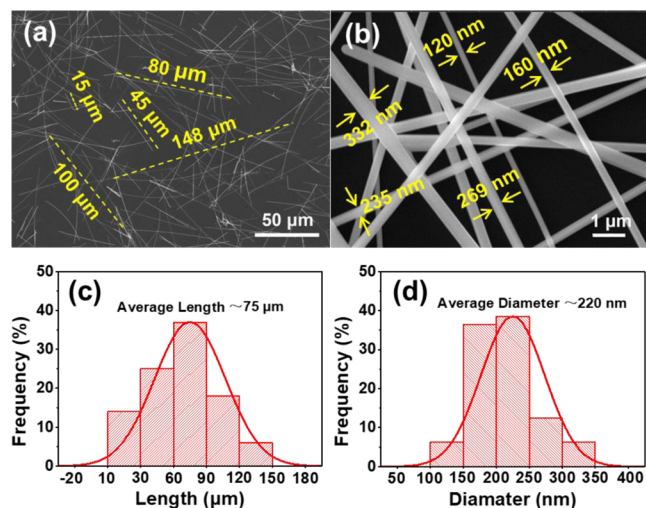


**Figure 1.** (a) SEM and (b) FESEM images of AgNWs synthesized in 1,2-PG at 393 K with a PVP/AgNO<sub>3</sub> mass ratio of 6%. (c, d) Statistic distribution of the length and diameter of AgNWs.

sample is composed of homogeneously distributed AgNWs with an average length of  $\sim 75 \mu\text{m}$ . Figure 1b,d exhibits the FESEM image and the statistic distribution of the diameter, which indicate that the AgNWs are composed of highly crystalline wires with an average diameter of  $\sim 220 \text{ nm}$ .

The structure and crystallinity of the synthesized AgNWs were determined by XRD. As shown in Figure 2, the five different peaks correspond to the (111), (200), (220), (311), and (222) planes of the face-centered cubic (fcc) structure of Ag (JCPDS card no. 99-0094). The intensity ratio of the reflections at [111] and [200] showed a high value, indicating that their {111} planes tended to be preferentially oriented.<sup>3</sup> In

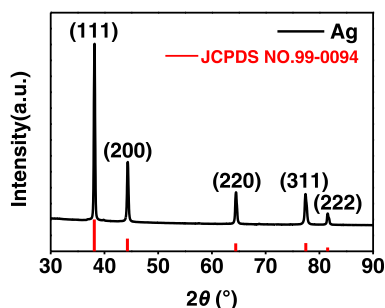


**Figure 2.** XRD pattern of AgNWs synthesized at 393 K with a PVP/AgNO<sub>3</sub> mass ratio of 6%.

addition, no other visible peaks were found in the XRD pattern, which confirmed the as-synthesized AgNWs with high crystallinity and purity.

**3.2. Possible Formation Mechanism of the Silver Nanowires.** To investigate the morphology evolution of AgNWs during the reaction, some samples were collected at different times of 4, 5, and 6 h during the synthesis of nanowires and analyzed by TEM and UV-vis. Figure 3a shows

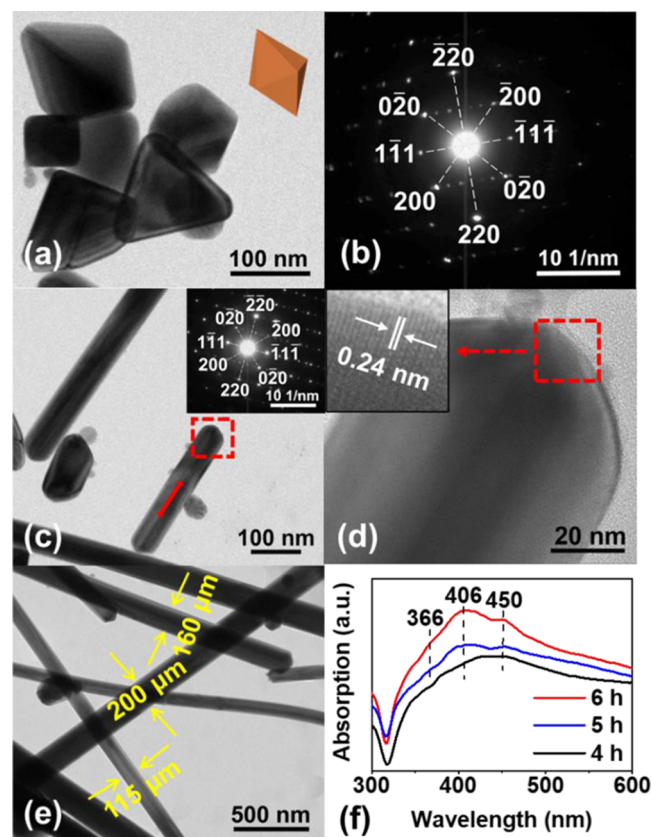


**Figure 3.** TEM images and UV-vis absorption spectra for samples collected from the reaction performed at 393 K in a closed reaction vessel for (a) 4, (c) 5, and (e) 6 h. (b) Typical selected-area electron diffraction (SAED) pattern recorded from the multiple twin particles in (a). (d) HRTEM image corresponding to the portion marked in red in (c). (f) UV-vis absorption spectra of products prepared at different stages.

the TEM image of decahedral multiple twinning Ag seeds with a penta-twinned structure generated at 4 h. The coexistence of a small number of Ag nano right bipyramids and Ag nanoplates in this sample might be produced by the etching of nitric acid and carboxylic acid. Figure 3b shows the typical selected-area electron diffraction (SAED) pattern recorded from multiple twin particles in Figure 3a. This pattern indicates that the nanoparticles are not a single crystal because diffraction spots do not match any particular patterns with face-centered cubic silver. It can be seen from Figure 3b that the pattern is composed of two independent rectangular diffraction patterns overlapping each other, which is symmetrical to the [001] zone axis and the  $\bar{1}22$  zone axis, respectively. The different orientations of these two zones induced the generation of double diffraction.<sup>24</sup> This pattern is consistent with the results obtained for pentagonal multiple twinned AgNWs.<sup>21</sup> As the reaction progressed, nanorods of different lengths were found

along with few nanoparticles after 5 h (Figure 3c). A twin plane of silver nanorods is revealed to be parallel to the longitudinal axis, as indicated by the arrow, meaning that the silver nanorods have a fivefold twinned structure consisting of five twinned subunits.<sup>25</sup> Also, the inset (SAED) of Figure 3c is consistent with the results obtained for pentagonal multiple twinned AgNWs. In Figure 3d, the HRTEM image showed clear lattice fringes with a d-spacing of about 0.24 nm, which is in good agreement with the  $d(111)$  spacing for SAED silver nanorods and confirmed that AgNWs have a fivefold twinned structure that grows along the [011] direction.<sup>26</sup> The nanorods grown into AgNWs in the sample (Figure 3e) are collected after 6 h. Also, the nanoparticles are very sparse in this sample. In addition, it is well known that the PVP will be wrapped on the surface of AgNWs under the action of Ag–O bonds; however, from Figure 3e, the layer was not found, which means that PVP was completely removed by washing.

Furthermore, the UV–vis absorption spectra were compared for the above three samples. As shown in Figure 3f, in which the peak at 366 nm corresponds to the plasmon response of AgNWs.<sup>27</sup> The 406 nm peak could be attributed to the transverse surface plasmon resonance of AgNWs,<sup>3</sup> whereas a shoulder around 450 nm may originate from the in-plane dipole resonance of Ag nanoplates and Ag nano right bipyramids.<sup>28–30</sup> When the reaction mixture was heated for 4 h, a broad characteristic peak centered at 430 nm was monitored, which is the characteristic peak that is considered to originate from Ag nanoparticles. At this time, the sample was likely composed of multiple twinned Ag seed particles, few Ag nano right bipyramids, and Ag nanoplates. After 5 h, a new peak at 366 nm was observed, together with a weak shoulder at 358 nm, characteristic of AgNW crystals, which illustrates that the small Ag seed particles have grown into Ag nanorods and nanowires. When the synthesis was completed after 6 h, a sharper and narrower peak at 406 nm could be identified for the sample; however, the characteristic peak at 450 nm became weaker, implying that these Ag nanorods have further grown into AgNWs.

In a typical polyol synthesis of AgNWs, 1,2-PG acts as both the medium and reducing agent for silver ions, and PVP acts as both a capping agent and dispersant. It is well known that 1,2-PG can be continuously oxidized to produce hydroxyacetone, methylglyoxal, and pyruvic acid under acidic conditions. The pyruvic acid will be further rapidly oxidized to acetic acid and formic acid (Figure 4).<sup>31,32</sup>

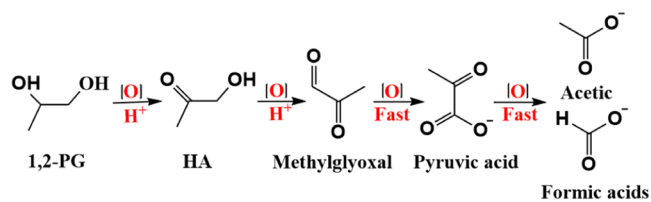


**Figure 4.** Reaction routes for the catalytic oxidation of 1,2-PG in an acidic solution.

To identify the change in the functional group of 1,2-PG after being oxidized by  $\text{Ag}^+$ , the pure 1,2-PG, 1,2-PG heated at a temperature of 393 K in a closed reaction vessel, and 1,2-PG oxidized by  $\text{Ag}^+$  at a temperature 393 K in a closed reaction vessel were analyzed by FTIR. As shown in Figure 5, in the case of pure 1,2-PG, the peak at  $3331\text{ cm}^{-1}$  is assigned to the

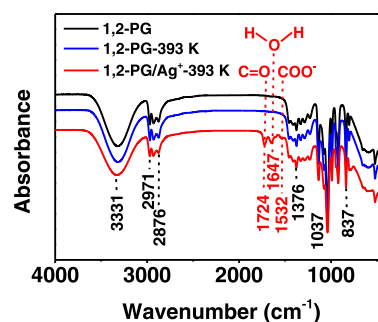


**Figure 5.** FTIR spectra for the pure 1,2-PG, 1,2-PG heated at 393 K, and 1,2-PG after reducing  $\text{Ag}^+$ .

stretching vibration of OH.<sup>33</sup> The peaks near  $2876$  and  $2971\text{ cm}^{-1}$  are related to CH asymmetric and symmetric stretching modes, respectively, while those at  $837$ – $1376\text{ cm}^{-1}$  are assigned to the CO stretching vibration.<sup>34,35</sup> It is worth noting that 1,2-PG has three characteristic peaks at  $1724$ ,  $1647$ , and  $1532\text{ cm}^{-1}$  after reducing  $\text{Ag}^+$ , respectively. The peaks near  $1724\text{ cm}^{-1}$  are the result of the carbonyl (C=O) stretching mode,<sup>36,37</sup> which indicates that hydroxyacetone or methylglyoxal was formed in the reaction of 1,2-PG and  $\text{Ag}^+$ . The peak around  $1647\text{ cm}^{-1}$  is due to the HOH bending mode frequency in liquid water, which suggested that water was formed in the reaction of 1,2-PG and  $\text{Ag}^+$ .<sup>38,39</sup> The presence of carboxylate groups was verified by the asymmetric ( $\text{COO}^-$ ) stretching at  $1532\text{ cm}^{-1}$ .<sup>40,41</sup> Its position confirms a binding of carboxylate oxygens to silver.<sup>42,43</sup> However, the 1,2-PG heated at a temperature of 393 K in a closed reaction vessel did not show the characteristic peak. This proves that  $\text{Ag}^+$  was the main oxidant in the 1,2-PG oxidation path. The FTIR results are in good agreement with Figure 4. Therefore, it can be concluded that the hydroxyacetone (HA) or methylglyoxal, water, and carboxylate were formed in the reaction of 1,2-PG and  $\text{Ag}^+$ . The low-boiling intermediate products HA ( $418\text{ K}$ ) and methylglyoxal ( $348\text{ K}$ ) were likely the main factors for the synthesis of AgNWs at low temperatures ( $393\text{ K}$ ).

Based on the experimental results discussed above, a possible growth mechanism of AgNWs was proposed. 1,2-Propanediol begins to undergo a continuous oxidation reaction when heated at specific temperatures (reaction 1). At the same time,  $\text{Ag}^+$  was continuously reduced into  $\text{Ag}^0$  atoms. When the concentration of  $\text{Ag}^0$  atoms in the liquid phase reaches supersaturation, the aggregated  $\text{Ag}^0$  nucleates grow into Ag seeds, which may be randomly composed of single crystal, polycrystalline nanoparticles, and multiply twinned particles (MTPs) with fivefold twinning decahedral structures. As is known, MTPs are preferentially formed due to its thermodynamically stable state, when concentration of free  $\text{Ag}^+$  ions is sufficiently low in the reaction.<sup>44,45</sup> Since the reaction vessel was closed, the formic acid ( $\text{CH}_3\text{COOH}$ ), acetic acid ( $\text{CH}_3\text{CH}_2\text{COOH}$ ), and nitric acid ( $\text{HNO}_3$ ) produced in reaction 1 could be kept inside the reactor in a reflux condition. The nitric acid can oxidize nanosilver into silver nitrate with the release of NO gas (reactions 2 and 3).<sup>9,44</sup> The carboxylic acid can oxidize nanosilver into silver carboxylate (reactions 4 and 5). Nitric acid and carboxylic acid act as strong etchants by redissolving some of the MTPs with surface defects, which results in the formation of a lower concentration of free  $\text{Ag}^+$  ions, which will further facilitate the formed nuclei to evolve into MTPs.<sup>9</sup> In addition, the closed reaction vessel

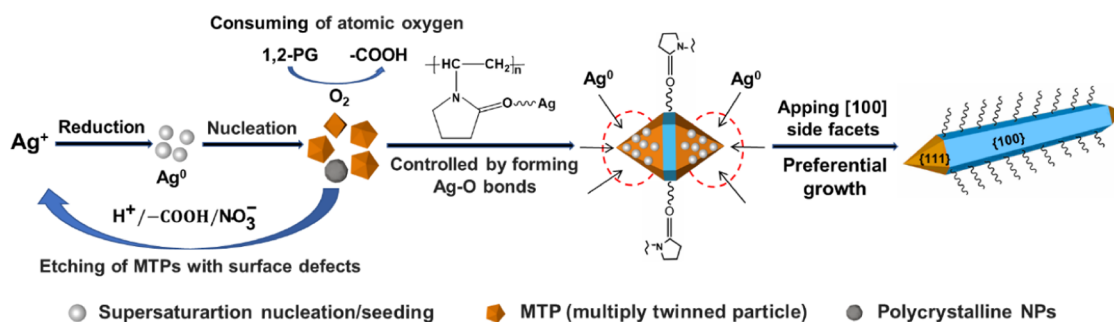


Figure 6. Reaction scheme for the formation of AgNWs.

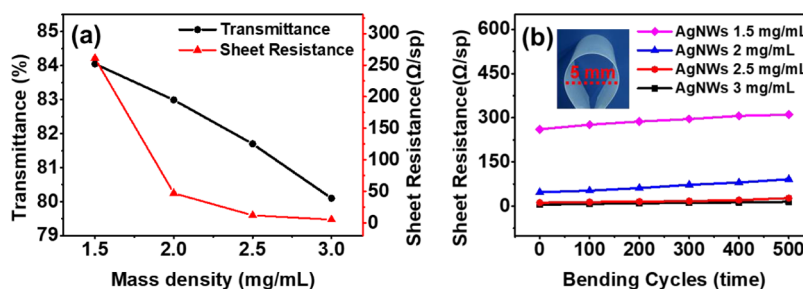
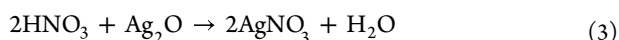
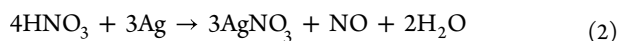
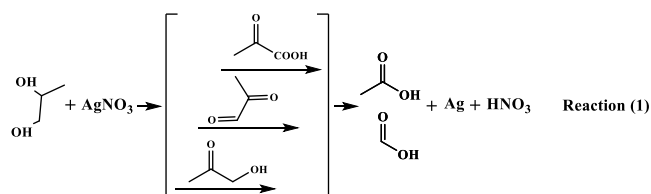


Figure 7. (a) Optical transmittance and sheet resistance for AgNW TCFs with different mass densities. (b) Sheet resistance change measurements during 500 bending cycles (5 mm bending radius) for AgNW TCFs with different mass densities. The inset shows the bent state of the AgNW TCF.

can avoid oxygen from being adsorbed on the [111] facets of MTPs, thus freeing these active sites for the deposition of more Ag atoms and longitudinal growth into AgNWs.<sup>9,46</sup> To promote unidirectional growth into nanowires, it can be controlled by surface capping agent PVP forming Ag–O bonds and preferentially covering the [100] facets of MTPs and promoting unidirectional growth by permitting Ag atoms to be deposited only on the [111] facets, as shown in Figure 6.



**3.3. Transmittance and Sheet Resistance Test of AgNW Transparent Conductive Films.** AgNWs transparent conductive films are a promising candidate to replace traditional indium tin oxide as the next-generation transparent and flexible electrode. However, the junction resistance between AgNWs greatly affects the conductivity of the nanowire network and largely overshadows the wide application of AgNWs. Lately, several studies have shown progress in reducing the junction resistance between AgNWs, such as annealing,<sup>47</sup> mechanical pressing,<sup>48</sup> chemical treatment,<sup>49</sup> and plasma welding.<sup>50</sup> The annealing and mechanical pressing are suitable for AgNW network electrodes on heat-

resistant substrates or rigid substrates. The chemical treatment is applicable to transparent conductive films with low transmittance requirements. Among them, plasma welding can realize the welding of AgNWs with minimal thermal influence. However, the focused laser spot will only weld nanowires in a small area irradiated by the spot laser, which has a limitation with respect to efficient large-scale processing.<sup>51</sup> Based on the existing laboratory infrastructure, low-temperature annealing was chosen in this study to reduce the junction resistance between AgNWs.

The prepared AgNWs have been used to make transparent conductive films by spin-coating method on the PET substrates and drying at a temperature of 393 K for 30 min. Figure 7a shows the effect of the AgNW mass ratio on the transmittance and sheet resistance of transparent conductive films (TCFs). It is obvious that the sheet resistance and transmittance are decreased due to the increase in the mass ratio of AgNWs. When the AgNW mass ratio was 2.5%, a very low resistance of 12.25 Ω/square and transmittance of 81.7% (92.36% for AgNW network only without substrate) were achieved (see Figure S3 in the Supporting Information). The resistance value is much lower than those of the AgNWs prepared using halide salts to our knowledge, i.e., a sheet resistance greater than 25 Ω/square at about 91% transmittance (see Table S2).<sup>3,10,52</sup> The mechanical stability of the fabricated AgNW films has been evaluated by a bending test. As shown in Figure 7b, the AgNW films have good flexibility with no significant change in the sheet resistance even after bending for 500 cycles with a bending radius of 5 mm (see the inset of Figure 7b). In addition, the AgNW TCFs still maintain a good optical transmittance (see Table S3). This means that the AgNW films have good stability under mechanical stress; such excellent flexibility demonstrates potential applications in flexible devices.

## 4. CONCLUSIONS

In conclusion, we report a kind of simple and high-yield synthesis strategy for AgNWs with no halide salts at a relatively low temperature of 393 K. Meanwhile, we have studied the reaction mechanism for the synthesis of AgNWs, viz., by the continuous oxidation reaction of 1,2-PG in a closed reaction vessel. The nitric acid and carboxylic acid generated in the 1,2-PG oxidation reaction were used as etchants to reduce the reduction rate of Ag ions, which will facilitate the formed nuclei to evolve into MTPs. PVP was another factor facilitating the synthesis of AgNWs. Multiple twinned nanoparticles will grow in the [110] orientation and eventually evolve into AgNWs under the interaction of the PVP macromolecule with the {100} planes. Finally, the as-synthesized AgNWs with a yield of up to ~90% in an average length of 75  $\mu\text{m}$  were used to fabricate AgNW TCFs, which achieved a resistance of 12.25  $\Omega/\text{square}$  with a transmittance of 81.7%. The AgNWs reported in this study have potential applications in the fields of optoelectronics, biological sensors, and nanomedicine.

## ■ ASSOCIATED CONTENT

### SI Supporting Information

The Supporting Information is available free of charge at <https://pubs.acs.org/doi/10.1021/acsomega.2c07164>.

SEM and FESEM images of AgNWs synthesized at different temperatures and with various PVP/AgNO<sub>3</sub> mass ratios. XRD patterns of AgNWs synthesized at 393 K with a PVP/AgNO<sub>3</sub> mass ratio of 6%. Transmittance and sheet resistance for AgNW TCFs (PDF)

## ■ AUTHOR INFORMATION

### Corresponding Author

Hongwei Yang – State Key Laboratory of Advance Technologies for Comprehensive Utilization of Precious Metals, Kunming Institute of Precious Metals, Kunming 650106, China; [orcid.org/0000-0002-0674-1024](https://orcid.org/0000-0002-0674-1024); Email: [nanolab@ipm.com.cn](mailto:nanolab@ipm.com.cn)

### Authors

Huaming Mao – State Key Laboratory of Advance Technologies for Comprehensive Utilization of Precious Metals, Kunming Institute of Precious Metals, Kunming 650106, China

Jie Chen – State Key Laboratory of Advance Technologies for Comprehensive Utilization of Precious Metals, Kunming Institute of Precious Metals, Kunming 650106, China

Linlin He – State Key Laboratory of Advance Technologies for Comprehensive Utilization of Precious Metals, Kunming Institute of Precious Metals, Kunming 650106, China

Zhengyang Fan – State Key Laboratory of Advance Technologies for Comprehensive Utilization of Precious Metals, Kunming Institute of Precious Metals, Kunming 650106, China

Yu Ren – State Key Laboratory of Advance Technologies for Comprehensive Utilization of Precious Metals, Kunming Institute of Precious Metals, Kunming 650106, China

Jungang Yin – State Key Laboratory of Advance Technologies for Comprehensive Utilization of Precious Metals, Kunming Institute of Precious Metals, Kunming 650106, China

Wei Dai – State Key Laboratory of Advance Technologies for Comprehensive Utilization of Precious Metals, Kunming Institute of Precious Metals, Kunming 650106, China

Complete contact information is available at: <https://pubs.acs.org/10.1021/acsomega.2c07164>

### Notes

The authors declare no competing financial interest.

## ■ ACKNOWLEDGMENTS

This work has been supported by the Scientific and Technological Projects of Yunnan Precious Metals Laboratory (Grant No. YPML-2022050201), the National Natural Science Foundation of China (Grant No. 21761016), the Major R&D Project of Yunnan Province (Grant Nos. 202002AB080001-1 and 202102AB080008-5), the Young and Middle-aged Academic and Technical Leaders Reserve Talents Program of Yunnan Province (Grant No. 2017HB060), and Ten Thousand Talents Plan-Young Top Talent Program of Yunnan Province (Grant No. 2019020001).

## ■ REFERENCES

- (1) Britton, J.; Krukiewicz, K.; Chandran, M.; Fernandez, J.; Poudel, A.; Sarasua, J. R.; FitzGerald, U.; Biggs, M. J. P. A flexible strain-responsive sensor fabricated from a biocompatible electronic ink via an additive-manufacturing process. *Mater. Des.* **2021**, *206*, No. 109700.
- (2) Liu, H.; Li, Y.; Wu, J.; Fu, Y. Y.; Tang, H.; Yi, X. T.; Xie, Z. Y. MEA surface passivation of a AgNWs: SnO<sub>2</sub> composite transparent electrode enables efficient flexible ITO-free polymer solar cells. *J. Mater. Chem. C* **2021**, *9*, 9914–9921.
- (3) Li, Y. X.; Li, Y.; Fan, Z. Y.; Yang, H. W.; Yuan, X. M.; Wang, C. Ascorbic acid-assisted one-step chemical reaction to design an ultralong silver nanowire structure for a highly transparent flexible conducting film. *ACS Omega* **2020**, *5*, 18458–18464.
- (4) Zhao, H. X.; Zhou, Y. L.; Cao, S. T.; Wang, Y. F.; Zhang, X. J.; Fang, S. X.; Wang, J. C.; Li, D. C.; Kong, D. S. Ulstretchable and washable conductive microtextiles by coassembly of silver nanowires and elastomeric microfibers for epidermal human–machine interfaces. *ACS Mater. Lett.* **2021**, *3*, 912–920.
- (5) De Mori, A.; Hafidh, M.; Mele, N.; Yusuf, R.; Cerri, G.; Gavini, E.; Tozzi, G.; Barbu, E.; Conconi, M.; R Draheim, R.; Roldo, M. Sustained release from injectable composite gels loaded with silver nanowires designed to combat bacterial resistance in bone regeneration applications. *Pharmaceutics* **2019**, *11*, 116–135.
- (6) Amjadi, M.; Pichitpajongkit, A.; Lee, S.; Ryu, S.; Park, I. Highly stretchable and sensitive strain sensor based on silver nanowire-elastomer nanocomposite. *ACS Nano* **2014**, *8* (5), 5154–5163.
- (7) Li, Y.; Yuan, X. M.; Yang, H. W.; Chao, Y. X.; Gou, S. L.; Wang, C. One-step synthesis of silver nanowires with ultra-long length and thin diameter to make flexible transparent conductive films. *Materials* **2019**, *12*, 401–412.
- (8) Yuan, X. M.; Yang, H. W.; Li, Y. X.; Li, Y.; Chao, Y. X.; Chen, J. L.; Chen, L. Synthesis of silver nanowires by using tetrabutyl ammonium dibromochloride as the auxiliary for low-haze flexible transparent conductive film. *Langmuir* **2019**, *35*, 11829–11835.
- (9) Patil, S.; Kate, P. R.; Deshpande, J. B.; Kulkarni, A. A. Quantitative understanding of nucleation and growth kinetics of silver nanowires. *Chem. Eng. J.* **2021**, *414*, 128711–128727.
- (10) Chen, C.; Zhao, Y.; Wei, W.; Tao, J.; Lei, G.; Jia, D.; Wan, M.; Li, S.; Ji, S.; Ye, C. Fabrication of silver nanowire transparent conductive films with an ultra-low haze and ultra-high uniformity and their application in transparent electronics. *J. Mater. Chem. C* **2017**, *5*, 2240–2246.
- (11) Gupta, R.; Rao, K. D. M.; Kiruthika, S.; Kiruthika, G. U. Visibly transparent heaters. *ACS Appl. Mater. Interfaces* **2016**, *8*, 12559–12575.
- (12) Lee, J.; Lee, I.; Kim, T. S.; Lee, J. Y. Efficient welding of silver nanowire networks without post-processing. *Small* **2013**, *9*, 2887–2894.

- (13) Hecht, D. S.; Hu, L.; Irvin, G. Emerging transparent electrodes based on thin films of carbon nanotubes, graphene, and metallic nanostructures. *Adv. Mater.* **2011**, *23*, 1482–1513.
- (14) Wu, H.; Hu, L. B.; Rowell, M. W.; Kong, D.; Cha, J. J.; McDonough, J. R.; Zhu, J.; Yang, Y.; McGehee, M. D.; Cui, Y. Electrospun metal nanofiber webs as high-performance transparent electrode. *Nano Lett.* **2010**, *10*, 4242–4248.
- (15) Zeng, X. Y.; Zhang, Q. K.; Yu, R. M.; Lu, C. Z. A new transparent conductor: silver nanowire film buried at the surface of a transparent polymer. *Adv. Mater.* **2010**, *22*, 4484–4488.
- (16) Lee, J. H.; An, K.; Won, P.; Ka, Y.; Hwang, H.; Moon, H.; Kwon, Y.; Hong, S.; Kim, C.; Lee, C.; Ko, S. W. A dual-scale metal nanowire network transparent conductor for highly efficient and flexible organic light emitting diodes. *Nanoscale* **2017**, *9*, 1978–1985.
- (17) Elechiguerra, J. L.; Larios-Lopez, L.; Liu, C.; Garcia-Gutierrez, D.; Camacho-Bragado, A.; Yacamán, M. J. Corrosion at the nanoscale: The case of silver nanowires and nanoparticles. *Chem. Mater.* **2005**, *17*, 6042–6052.
- (18) Langle, D. P.; Lagrange, M.; Giusti, G.; Jiménez, C.; Bréchet, Y.; Nguyen, N. D.; Bellet, D. Metallic nanowire networks: Effects of thermal annealing on electrical resistance. *Nanoscale* **2014**, *6*, 13535–13543.
- (19) Liu, C. H.; Yu, X. Silver nanowire-based transparent, flexible, and conductive thin film. *Nanoscale Res. Lett.* **2011**, *6*, No. 75.
- (20) Wu, W. H.; Chuang, H. Y.; Hsu, S. L. Synthesis and mechanism of template-free growth of silver nanowires via syringes. *J. Mater. Res.* **2016**, *31*, 109–116.
- (21) Jia, C.; Yang, P.; Zhang, A. Glycerol and ethylene glycol mediated synthesis of uniform multiple crystalline silver nanowires. *Mater. Chem. Phys.* **2014**, *143*, 794–800.
- (22) Cong-Wen, X.; Hai, T. Y.; Cheng, M. S.; Li, Z. A.; Zhang, H. R.; Liu, F.; Yang, T. Z.; Chen, S. T.; Gao, H. J. Controlled growth of large-scale silver nanowires. *Chin. Phys.* **2005**, *14*, 2269–2275.
- (23) Madeira, A.; Papanastasiou, D. T.; Toupance, T.; Servant, L.; Treguer-Delapierre, M.; Bellet, D.; Goldthorpe, I. Rapid synthesis of ultra-long silver nanowires for high performance transparent electrodes. *Nanoscale Adv.* **2020**, *2*, 3804–3808.
- (24) Sun, Y.; Mayers, B.; Herricks, T.; Xia, Y. Polyol synthesis of uniform silver nanowires: a plausible growth mechanism and the supporting evidence. *Nano Lett.* **2003**, *3*, 955–960.
- (25) Niu, Z.; Cui, F.; Kuttner, E.; Xie, C.; Chen, H.; Sun, Y.; Dehestani, A.; Schierle-Arndt, K.; Yang, P. Synthesis of silver nanowires with reduced diameters using benzoin-derived radicals to make transparent conductors with high transparency and low haze. *Nano Lett.* **2018**, *18*, 5329–5334.
- (26) Fahad, S.; Yu, H.; Wang, L.; Zain-ul-Abdin; Haroon, M.; Ullah, R. S.; Nazir, A.; Naveed, K.; Elshaarani, T.; Khan, A. Recent progress in the synthesis of silver nanowires and their role as conducting materials. *J. Mater. Sci.* **2019**, *54*, 997–1035.
- (27) da Silva, R. R.; Yang, M.; Choi, S. I.; Chi, M.; Luo, M.; Zhang, C.; Li, Z. Y.; Camargo, P. H. C.; Ribeiro, S. J. L.; Xia, Y. Facile synthesis of sub-20 nm silver nanowires through a bromide-mediated polyol method. *ACS Nano* **2016**, *10*, 7892–7900.
- (28) Xiong, Y. J.; Siekkinen, A. R.; Wang, J. G.; Yin, Y. D.; Kim, M. J.; Xia, Y. N. Synthesis of silver nanoplates at high yields by slowing down the polyol reduction of silver nitrate with polyacrylamide. *J. Mater. Chem.* **2007**, *17*, 2600–2602.
- (29) Zhang, J.; Langille, M. R.; Mirkin, C. A. Photomediated synthesis of silver triangular bipyramids and prisms: the effect of pH and BSP. *J. Am. Chem. Soc.* **2010**, *132*, 12502–12510.
- (30) Tsuji, M.; Maeda, Y.; Hikino, S.; Kumagai, H.; Matsunaga, M.; Tang, X. L.; Matsuo, R.; Ogino, M.; Jiang, P. Shape evolution of octahedral and triangular platelike silver nanocrystals from cubic and right bipyramidal seeds in DMF. *Cryst. Growth Des.* **2009**, *9*, 4700–4705.
- (31) Dimitratos, N.; Lopez-Sanchez, J. A.; Meenakshisundaram, S.; Anthonykutty, J. M.; Brett, G.; Carley, A. F.; Taylor, S. H.; Knight, D. W.; Hutchings, G. J. Selective formation of lactate by oxidation of 1, 2-propanediol using gold palladium alloy supported nanocrystals. *Green Chem.* **2009**, *11*, 1209–1216.
- (32) Feng, Y.; Lu, C.; Wang, H.; Meng, M.; Zhang, Y.; Rao, D.; Liu, L.; Yin, H. Spinel copper-iron-oxide magnetic nanoparticles with cooperative Cu (i) and Cu (ii) sites for enhancing the catalytic transformation of 1, 2-propanediol to lactic acid under anaerobic conditions. *Catal. Sci. Technol.* **2020**, *10*, 8094–8107.
- (33) Tong, J.; Zhang, H.; Gu, J.; Li, L.; Ma, C.; Zhao, J.; Wang, C. Y. Poly (ethylene glycol)-block-poly (propylene glycol)-block-poly (ethylene glycol)-assisted synthesis of graphene/polyaniline composites as high-performance supercapacitor electrodes. *J. Mater. Sci.* **2016**, *51*, 1966–1977.
- (34) Levang, A. K.; Zhao, K.; Singh, J. Effect of ethanol/propylene glycol on the in vitro percutaneous absorption of aspirin, biophysical changes and macroscopic barrier properties of the skin. *Int. J. Pharm.* **1999**, *181*, 255–263.
- (35) Tomishige, K.; Yasuda, H.; Yoshida, Y.; Nurunnabi, M.; Li, B.; Kunimori, K. Novel route to propylene carbonate: selective synthesis from propylene glycol and carbon dioxide. *Catalysis Lett.* **2004**, *95*, 45–49.
- (36) Gordon, B. P.; Moore, F. G.; Scatena, L. F.; Valley, N. A.; Wren, S. N.; Richmond, G. L. Model behavior: characterization of hydroxyacetone at the air–water interface using experimental and computational vibrational sum frequency spectroscopy. *J. Phys. Chem. A* **2018**, *122*, 3837–3849.
- (37) Sharma, A.; Reva, I.; Fausto, R.; Hesse, S.; Xue, Z. F.; Suhm, M. A.; Nayak, S. K.; Sathishkumar, R.; Pal, R.; Row, T. N. G. Conformation-changing aggregation in hydroxyacetone: a combined low-temperature FTIR, jet, and crystallographic study. *J. Am. Chem. Soc.* **2011**, *133*, 20194–20207.
- (38) Vinaykin, M.; Benderskii, A. V. Vibrational sum-frequency spectrum of the water bend at the air/water interface. *J. Phys. Chem. Lett.* **2012**, *3*, 3348–3352.
- (39) Nagata, Y.; Hsieh, C. S.; Hasegawa, T.; Voll, J.; Backus, E. H. G.; Bonn, M. Water bending mode at the water–vapor interface probed by sum-frequency generation spectroscopy: a combined molecular dynamics simulation and experimental study. *J. Phys. Chem. Lett.* **2013**, *4*, 1872–1877.
- (40) Ibrahim, M.; Nada, A.; Kamal, D. E. Density functional theory and FTIR spectroscopic study of carboxyl group. *Indian J. Pure Appl. Phys.* **2005**, *43*, 911–917.
- (41) Liao, L. F.; Lien, C. F.; Lin, J. L. FTIR study of adsorption and photoreactions of acetic acid on TiO<sub>2</sub>. *Phys. Chem. Chem. Phys.* **2001**, *3*, 3831–3837.
- (42) Du, J.; Sun, X. Y.; He, Y. C.; Yu, Y.; Zheng, X. F.; Tian, L. J.; Liu, Z. The proton conductivities of two silver-thiophene-2-carboxylate coordination polymer and the relationship between the dimensionality and property. *Appl. Organomet. Chem.* **2018**, *32*, e4517–e4526.
- (43) Uznanski, P.; Bryszewska, E. Synthesis of silver nanoparticles from carboxylate precursors under hydrogen pressure. *J. Mater. Sci.* **2010**, *45*, 1547–1552.
- (44) Parente, M.; Van Helvert, M.; Hamans, R. F.; Verbroekken, R.; Sinha, R.; Bieberle-Hutter, A.; Baldi, A. Simple and fast high-yield synthesis of silver nanowires. *Nano Lett.* **2020**, *20*, 5759–5764.
- (45) Bari, B.; Lee, J.; Jang, T.; Won, P.; Ko, S. H.; Alamgir, K.; Arshadd, M.; Guo, L. G. Simple hydrothermal synthesis of very-long and thin silver nanowires and their application in high quality transparent electrodes. *J. Mater. Chem. A* **2016**, *4*, 11365–11371.
- (46) Bergin, S. M.; Chen, Y.-H.; Rathmell, A. R.; Charbonneau, P.; Li, Z.-Y.; Wiley, B. J. The effect of nanowire length and diameter on the properties of transparent, conducting nanowire films. *Nanoscale* **2012**, *4*, 1996–2004.
- (47) Hu, L.; Kim, H. S.; Lee, J. Y.; Peumans, P.; Cui, Y. Scalable coating and properties of transparent, flexible, silver nanowire electrodes. *ACS Nano* **2010**, *4*, 2955–2963.
- (48) Chung, C. H.; Song, T. B.; Bob, B.; Zhu, R.; Yang, Y. Solution processed flexible transparent conductors composed of silver

nanowire networks embedded in indium tin oxide nanoparticle matrices. *Nano Res.* **2012**, *5*, 805–814.

(49) Lu, H.; Zhang, D.; Cheng, J.; Liu, J.; Mao, J.; Choy, W. C. H. Optoelectronics: locally welded silver nano-network transparent electrodes with high operational stability by a simple alcohol-based chemical approach. *Adv. Funct. Mater.* **2015**, *25*, 4174.

(50) Lee, J.; Lee, P.; Lee, H.; Lee, D.; Lee, S. S.; Ko, S. H. Very long ag nanowire synthesis and its application in a highly transparent, conductive and flexible metal electrode touch panel. *Nanoscale* **2012**, *4*, 6408–6414.

(51) Song, T. B.; Chen, Y.; Chung, C. H.; Yang, Y.; Bob, B.; Duan, H. S.; Li, G.; Tu, K. N.; Huang, Y.; Yang, Y. Nanoscale joule heating and electromigration enhanced ripening of silver nanowire contacts. *ACS Nano* **2014**, *8*, 2804–2811.

(52) Jiu, J.; Araki, T.; Wang, J.; Nogi, M.; Sugahara, T.; Nagao, S.; Koga, H.; Suganuma, K.; Nakazawa, E.; Hara, M.; Uchida, H.; Shinozaki, K. Facile synthesis of very-long silver nanowires for transparent electrodes. *J. Mater. Chem. A* **2014**, *2*, 6326–6330.